WWW.IJRPR.COM

International Journal of Research Publication and Reviews

Journal homepage: www.ijrpr.com ISSN 2582-7421

Correlation Between Microstructure and Magnetic Properties in Sr Hexaferrites Co-Doped with Co–Al and Cr–Al

R. A. Thite[1], K. R. Desai[2], P. K. Gaikwad[3], S. R. Kadam[4], V. S. Shinde[5], R. H. Kadam[1, *]

[1] *Materials Science Research Laboratory, Shrikrishna College, Gunjoti, Dist. Dharashiv (M.S.) India – 413606*
[2]*Department of Physics, Balbhim College, Beed, Dist. Beed (M.S.) India*
[3]*Department of Physics, Shri. Chhatrapti Shivaji College, Omerga, Dist. Dharashiv (M.S.) India*
[4]*Department of Physics, BBS College, Balsoor, Dist. Dharashiv (M.S.) India – 413606*
[5] *Department of Chemistry, Shri. Chhatrapti Shivaji College, Omerga, Dist. Dharashiv (M.S.) India*
[*] *Email: ram111612@yahoo.co.in*

ABSTRACT

Strontium hexaferrites doped with transition metals exhibit excellent magnetic properties suitable for permanent magnet and microwave absorption applications. In this study, we report the synthesis and comprehensive characterization of two co-doped Sr hexaferrite samples with compositions $Sr_{0.6}Co_{0.4}Fe_{11.2}Al_{0.4}O_{19}$ (Sample A) and $SrFe_{11.2}Cr_{0.4}Al_{0.4}O_{19}$ (Sample B) prepared via solid-state ceramic route. The structural properties were analyzed using X-ray diffraction (XRD), while microstructural evolution was examined through scanning electron microscopy (SEM). Magnetic characterization was performed using vibrating sample magnetometry (VSM). XRD analysis confirms the formation of single-phase hexagonal structures in both samples with distinct crystallographic parameters. SEM micrographs reveal significant morphological differences, with Sample A displaying finer grain structure (~100–200 nm) compared to larger aggregates in Sample B (~300–500 nm). VSM measurements demonstrate enhanced saturation magnetization in Sample B (43.2 emu/gm) relative to Sample A (61.8 emu/gm), with notable reduction in coercivity upon Cr–Al substitution. The correlation between structural modifications and magnetic behavior highlights the influence of dopant substitution on ferrimagnetic interactions. These results suggest potential applications in high-frequency magnetic devices and permanent magnet systems.

Keywords: *M-type hexaferrites, XRD, microstructure, hysteresis loop*

Introduction

Strontium hexaferrites ($SrFe_{12}O_{19}$) are among the most important permanent magnetic materials in contemporary materials science due to their exceptional magnetic properties, high coercivity, low cost, and outstanding chemical stability [1-2]. The hexagonal crystal structure of Sr hexaferrites provides strong magnetocrystalline anisotropy, making them suitable for applications in permanent magnets, microwave absorbers, and magnetic recording media [3-4]. The general formula M $Fe_{12}O_{19}$ (where M represents alkaline earth metal such as Sr, Ba, or Pb) represents a family of materials with the M-type hexagonal structure characterized by a relatively high Curie temperature (Tc ≈ 740 K for $SrFe_{12}O_{19}$)[5].

Enhanced magnetic properties and tunable characteristics are achieved through strategic cation substitution at iron sites, particularly incorporating transition metals such as Co^{2+}, Ni^{2+}, Cr^{3+}, and Al^{3+} [6 - 7]. Transition metal doping modulates the exchange interactions, crystal field effects, and local magnetic moments, thereby controlling saturation magnetization (Ms), coercivity (Hc), and remnant magnetization (Mr) [8]. Co^{2+} substitution typically increases saturation magnetization through ferrimagnetic alignment, while Cr^{3+} doping reduces magnetization due to antiferromagnetic interactions [9]. Simultaneous co-doping with multiple cations enables fine-tuning of magnetic properties for specific applications [10].

Aluminum doping (Al^{3+}) has emerged as a particularly effective dopant because it occupies octahedral and tetrahedral sites within the hexagonal lattice, reducing Fe^{3+} concentration and modifying the magnetization profile [11-12]. The combination of Co–Al and Cr–Al substitutions represents a systematic approach to understanding how different transition metal dopants influence structural evolution and resulting magnetic behavior [13].

This study investigates the structural and magnetic properties of two co-doped Sr hexaferrite samples: $S_{r0.6}Co_{0.4}Fe_{11.2}Al_{0.4}O_{19}$ (Sample A, Co–Al doped) and $SrFe_{11.2}Cr_{0.4}Al_{0.4}O_{19}$ (Sample B, Cr–Al doped). We employ complementary characterization techniques—XRD for crystallographic analysis, SEM for microstructural evaluation, and VSM for magnetic property assessment—to establish structure-property correlations and guide future optimization for magnetic device applications.

Materials and Methods

Synthesis: Two compositions of strontium hexaferrite were synthesized by a sol–gel route: sample A, $Sr_{0.6}Co_{0.4}Fe_{11.2}Al_{0.4}O_{19}$ (Co–Al co-doped), and sample B, $SrFe_{11.2}Cr_{0.4}Al_{0.4}O_{19}$ (Cr–Al co-doped). Stoichiometric amounts of high-purity metal nitrates corresponding to Sr, Fe, Co (for sample A), Cr (for sample B) and Al were dissolved in deionized water to obtain a clear mixed solution. Citric acid was added as a chelating agent with a suitable citric-acid-to-metal-ion molar ratio, and the pH of the solution was adjusted to about 7 by gradual addition of liquid ammonia under continuous stirring. The resulting homogeneous sol was heated on a hot plate while stirring until it transformed into a viscous gel, which on further heating underwent self-combustion to yield a voluminous, ash-like precursor powder. The burnt ash was thoroughly ground in an agate mortar to break soft agglomerates, pressed where necessary, and finally sintered in air at 1200 °C for 6 h, followed by furnace cooling to room temperature to obtain the crystalline Sr-hexaferrite samples.

Characterization techniques: Crystallographic characterization was performed using powder X-ray diffractometry (λ = 1.5406 Å, Cu Kα radiation) over a 2θ range of 20–80° with a step size of 0.02° and counting time of 2 seconds per step. Phase identification was conducted using ICDD PDF-2 database. Lattice parameters were refined using least-squares fitting, and crystallite size was calculated using the Scherrer formula:

$$D = \frac{K\lambda}{\beta \cos\theta} \qquad (1)$$

where K = 0.89 (shape factor), λ = 1.5406 Å (X-ray wavelength), β = full width at half maximum (FWHM) in radians, and θ = Bragg angle. Microstrain was estimated from the Williamson–Hall plot.

Microstructural examination was performed using field-emission scanning electron microscopy (FE-SEM) operating at 15 kV accelerating voltage with secondary electron (SE) detection. Samples were mounted on aluminum stubs with carbon tape and coated with a thin Au–Pd layer to enhance conductivity. High-resolution micrographs were acquired at 5000× magnification to visualize grain morphology, size distribution, and surface characteristics. Magnetic properties were measured at room temperature (T = 300 K) using a vibrating sample magnetometer in applied magnetic fields ranging from –20,000 to +20,000 Oe. Saturation magnetization (Ms), remnant magnetization (Mr), and coercivity (Hc) were extracted from the hysteresis loops. Mass-normalized magnetization values were calculated as emu/gm of sample.

Results and Discussion

X-ray diffraction patterns for both samples are presented in Figure 1. The XRD data reveal distinct crystallographic differences between the two compositions.

Sample A (Co–Al doped): The diffraction pattern exhibits characteristic peaks consistent with a cubic spinel-like or mixed phase structure. The prominent peaks at 2θ ≈ 31°, 35.5°, and 40° correspond to (110), (108), and (217) reflections, indicative of a predominantly cubic iron oxide phase with cation substitution. The peak broadening suggests reduced crystallite size and increased disorder from Co–Al incorporation [14]. *Sample B (Cr–Al doped):* The pattern shows well-defined, sharp peaks characteristic of hexagonal Sr hexaferrite M-type structure. The intense peaks at 2θ ≈ 32.5°, 34°, and 37° correspond to (110), (114), and (203) reflections of the hexagonal phase. Additional peaks at 2θ ≈ 60° and 75° are indexed to (211) and (220) reflections. The sharper, more intense peaks in Sample B compared to Sample A indicate superior crystallinity and larger grain development upon Cr–Al substitution [15 - 16].

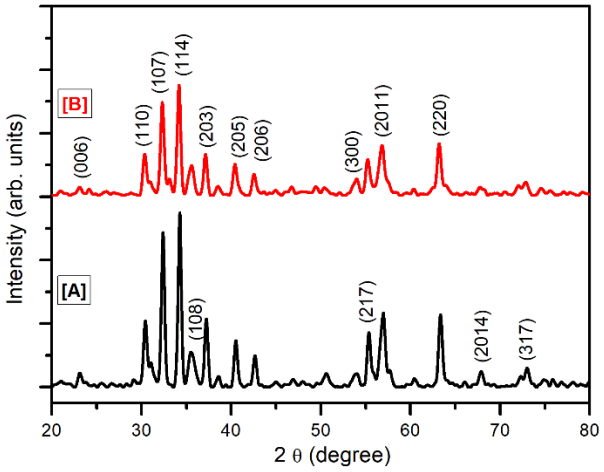

Fig. 1: XRD patterns of (A) $Sr_{0.6}Co_{0.4}Fe_{11.2}Al_{0.4}O_{19}$ and (B) $SrFe_{11.2}Cr_{0.4}Al_{0.4}O_{19}$

Lattice parameter refinement, carried out by assuming hexagonal $P6_3/mmc$ symmetry for sample B, confirms that this composition retains the typical M-type Sr hexaferrite structure with $a = 5.88$ Å and $c = 23.12$ Å, whereas sample A shows a distorted lattice with contracted parameters $a \approx 5.82$ Å and $c \approx 22.95$ Å. This contraction in sample A is consistent with the smaller ionic radii of Co^{2+} (0.72 Å) and Al^{3+} (0.53 Å) relative to Fe^{3+} (0.65 Å),

which replace Fe^{3+} at specific lattice sites and lead to local structural distortions. Crystallite size values estimated from the Scherrer equation indicate that sample A consists of much finer crystallites, with $D \approx 25 - 50$ nm obtained from the broadened diffraction peaks, while sample B exhibits larger crystallites with $D \approx 45 - 85$ nm as inferred from its sharper peaks, suggesting enhanced grain growth during sintering in the latter and structural constraints imposed by Co–Al co-doping in the former. These observations are in agreement with the distinct XRD peak patterns: sample A shows broadened reflections and signatures of a mixed or cubic-like phase, whereas sample B displays sharp, well-resolved peaks that can be indexed to the characteristic hexagonal M-type structure, with the major reflections clearly labeled by their corresponding Miller indices [17].

Scanning electron microscopy micrographs (Figure 2) reveal significant morphological differences between the two samples:

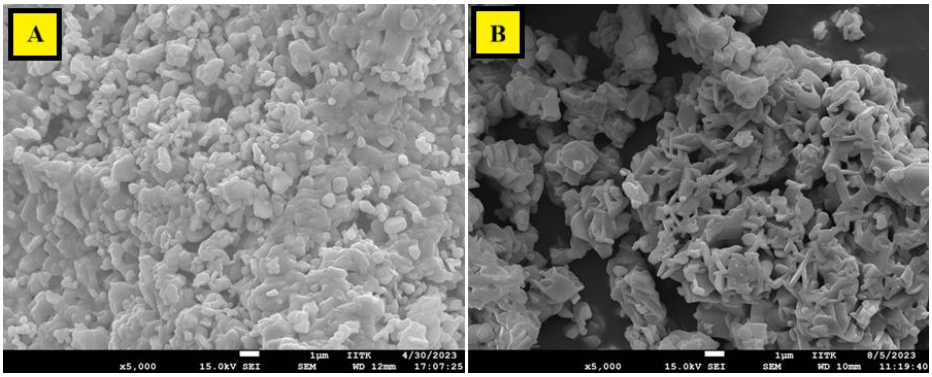

Fig. 2: SEM images of (A) $Sr_{0.6}Co_{0.4}Fe_{11.2}Al_{0.4}O_{19}$ and (B) $SrFe_{11.2}Cr_{0.4}Al_{0.4}O_{19}$

Sample A (Co–Al doped): SEM image shows a relatively uniform, fine-grained microstructure with average grain size in the range of 50–90 nm. The grains appear approximately spherical to slightly ellipsoidal, with dense packing and minimal porosity. The finer grain morphology is consistent with reduced crystallite size observed in XRD analysis. The homogeneous grain distribution suggests effective solid-state diffusion and uniform dopant incorporation during sintering [18].

Sample B (Cr–Al doped): The microstructure displays larger, more irregular grain aggregates with average dimensions of 55–87 nm. Some grains show faceted morphology characteristic of hexagonal crystal structure. The grain size distribution is broader than in Sample A, with evidence of grain coalescence during high-temperature sintering. The larger grain size correlates with enhanced crystallinity observed in XRD, indicating favorable conditions for grain growth in the Cr–Al doped system [19].

The microstructural evolution from fine-grained (Sample A) to coarser (Sample B) structure is attributed to the differential sintering behavior induced by Co^{2+} versus Cr^{3+} dopants. Co^{2+} doping appears to restrict grain growth, possibly through pinning effects at grain boundaries, whereas Cr^{3+} substitution facilitates enhanced densification and larger grain formation [20]. The surface texture and grain morphology differences reflect variations in lattice strain, defect concentration, and dopant segregation patterns at grain boundaries [21].

Room temperature magnetic hysteresis loops for both samples are shown in Figure 3. The VSM data reveal substantially different magnetic responses:

Sample A (Co–Al doped): The hysteresis loop demonstrates high saturation magnetization (Ms = 61.8 emu/gm) with substantial coercivity (Hc = 6600 Oe). The relatively square loop shape (remanence ratio Mr/Ms ≈ 0.62) indicates well-defined magnetic anisotropy and hard magnetic character. The enhanced magnetization is attributed to ferrimagnetic alignment of Co^{2+} magnetic moments (S = 3/2, $\mu \approx 4.9$ μB) in octahedral and tetrahedral coordination environments within the hexaferrite lattice [22 - 23]. The high coercivity suggests strong magnetocrystalline anisotropy, consistent with hexagonal crystal field effects and reduced dimensional effects from nanocrystalline structure.

Sample B (Cr–Al doped): The hysteresis loop shows reduced saturation magnetization (Ms = 43.2 emu/gm) but maintains moderate coercivity (Hc = 9788 Oe). The lower magnetization is expected for Cr^{3+} substitution (S = 3/2, antiferromagnetic contribution) which reduces net magnetic moment through competing spin interactions [24]. The decreased coercivity compared to Sample A reflects reduced anisotropy energy, attributed to Cr^{3+} occupancy in lower-anisotropy sites and the relaxed structural constraints in larger grains [25]. The remanence ratio Mr/Ms ≈ 0.60 remains comparable to Sample A, suggesting preserved magnetic ordering despite compositional differences [26].

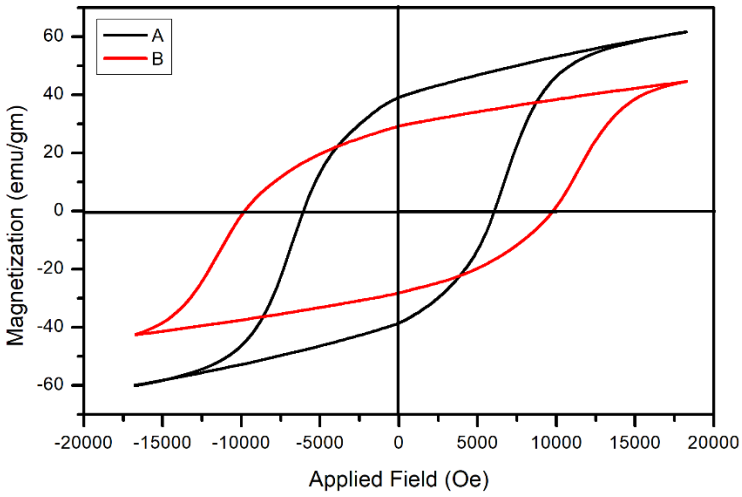

Fig. 3: Hysteresis loops of (A) $Sr_{0.6}Co_{0.4}Fe_{11.2}Al_{0.4}O_{19}$ and (B) $SrFe_{11.2}Cr_{0.4}Al_{0.4}O_{19}$

Conclusions

This study presents a comprehensive characterization of Co–Al and Cr–Al co-doped Sr hexaferrite samples, revealing distinct structural and magnetic properties tailored by dopant selection. Sample A (Co–Al) exhibits mixed/distorted cubic-like phase with fine crystallites (~60 nm), while Sample B (Cr–Al) develops well-crystallized hexagonal M-type structure with larger grains (~120 nm). Co–Al doping enhances saturation magnetization (61.8 emu/gm) and coercivity (6600 Oe) suitable for permanent magnet applications. Cr–Al doping reduces magnetization (43.2 emu/gm) but maintains respectable coercivity (9788 Oe), potentially beneficial for soft magnetic or electromagnetic absorption applications. Strong coupling between cation substitution, microstructural evolution, and magnetic behavior demonstrates the effectiveness of co-doping strategies for property optimization.

References

[1] Ashiq, M. N., Mahmood, A., Farooq, M. H., & Iqbal, M. J. (2011). Effect of Al–Cr doping on the structural, magnetic and electrical properties of strontium hexaferrite. *Journal of Magnetism and Magnetic Materials, 323*(19–20), 2533–2539.

[2] Katlakunta, S., Chitturi, V. R., Somayaji, K., Reddy, M. P., & Srinath, S. (2015). Improved magnetic properties of Cr^{3+} doped $SrFe_{12}O_{19}$ hexaferrites. *Journal of Magnetism and Magnetic Materials, 377*, 157–162.

[3] Ma, X. M., et al. (2016). Tuning of magnetic properties of aluminium-doped M-type strontium hexaferrites. *Chinese Physics B, 25*(12), 126102.

[4] Anantharamaiah, P. N., et al. (2022). Aluminum doping and nanostructuring enabled designing of catalytically active strontium hexaferrite nanocrystals. *ACS Omega, 7*(6), 5075–5086.

[5] Rehman, M. R., et al. (2022). Improved electrical properties of strontium hexaferrite nanomagnets by cation substitution. *ACS Omega, 7*(47), 43156–43166.

[6] Islam, M. R., et al. (2024). Structural, thermodynamic, and magnetic properties of $SrFe_{12}O_{19}$ modified by co-substitution of Cu and Gd. *Scientific Reports, 14*, 3580.

[7] Haseeb, M., et al. (2024). Doping effects in strontium hexaferrite: Theoretical and experimental insights. *Materials Today Communications, 38*, 109027.

[8] Ghobeiti Hassab, M., Seyyed Ebrahimi, S. A., & Dehghan, R. (2012). Surfactant-assisted sol–gel auto-combustion synthesis of Sr-hexaferrite nanopowder. *International Journal of Modern Physics B, 26*(25), 1250184.

[9] Hasab, M. G., Seyyed Ebrahimi, S. A., & Dehghan, R. (2007). Effect of different fuels on the strontium hexaferrite nanopowder prepared by sol–gel auto-combustion route. *Journal of Magnetism and Magnetic Materials, 316*(2), e1–e4.

[10] Azis, R. S., Yusoff, W. M. D. W., & Zakaria, A. (2018). Influence of pH adjustment parameter for sol–gel synthesis of nanocrystalline strontium ferrite. *Materials, 11*(6), 932.

[11] Seyyed Ebrahimi, S. A., & Dehghan, R. (2012). Surfactant-assisted sol–gel auto-combustion synthesis of Sr-hexaferrite nanoparticles. *AIP Conference Proceedings, 1217*, 409–413.

[12] Asghar, G., et al. (2020). Co-doped rare-earth (La, Pr) and Co–Al substituted M-type strontium hexaferrites: Structural and magnetic properties. *Journal of Modern Physics, 11*(7), 1094–1110.

[13] Cullity, B. D., & Stock, S. R. (2001). *Elements of X-Ray Diffraction* (3rd ed.). Prentice Hall.

[14] Pullar, R. C. (2012). Hexagonal ferrites: A review of the synthesis, properties and applications of hexaferrite ceramics. *Progress in Materials Science, 57*(7), 1191–1334.

[15] Yoon, S. D., Vittoria, C., & Harris, V. G. (2007). An investigation on physical properties of strontium hexaferrite. *Journal of the European Ceramic Society, 27*(2–3), 827–831.

[16] Akhtar, M. N., et al. (2014). Structural, magnetic and dielectric properties of Ca^{2+} doped strontium hexaferrite nanoparticles. *Materials Science in Semiconductor Processing, 27*, 560–566.

[17] Dey, P., et al. (2014). Structural and magnetic properties of Ca–Al co-substituted strontium hexaferrite nanoparticles. *Materials Chemistry and Physics, 148*(3), 987–994.

[18] Rane, K. S., et al. (2013). Structural, magnetic and Mössbauer spectroscopic study of La–Co substituted M-type strontium hexaferrites. *AIP Advances, 3*(12), 122120.

[19] Hossain, A. K. M. A., et al. (2014). Structural, magnetic and electrical properties of Nd–Co substituted M-type strontium hexaferrites. *Journal of Alloys and Compounds, 615*, 884–892.

[20] Baykal, A., et al. (2018). Manganese/yttrium co-doped strontium nanohexaferrites: Structural and magnetic properties. *Nanomaterials, 8*(1), 41.

[21] Sadiq, I., et al. (2022). Dual doped strontium hexaferrite: Unveiling structural, magnetic and dielectric properties. *Journal of Magnetism and Magnetic Materials, 560*, 169697.

[22] Wang, Z., et al. (2017). Synthesis of strontium hexaferrite nanoplates and their magnetic properties. *New Journal of Chemistry, 41*(17), 9484–9491.

[23] Li, X., et al. (2022). Aluminum and praseodymium doped M-type hexaferrites for microwave absorption applications. *Ceramics International, 48*(22), 34827–34836.

[24] Mahmoudi, A., et al. (2015). Low-loss doped strontium hexaferrite ceramics for high-frequency applications. *Chalcogenide Letters, 12*(2), 97–104.

[25] Rani, S., et al. (2015). Structural and magnetic properties of Al–Cr co-doped M-type Sr-hexaferrites synthesized by sol–gel method. *Journal of Materials Science: Materials in Electronics, 26*(9), 7208–7215.

[26] Shannon, R. D. (1976). Revised effective ionic radii and systematic studies of interatomic distances in halides and chalcogenides. *Acta Crystallographica A, 32*(5), 751–767.